

## Introduction

Objective mapping of image findings to the underlying anatomy is becoming an essential capability for functional neuroimaging. In the case of Diffuse Optical Tomography (DOT), complicating the goal of mapping activation findings to brain anatomy is the need for a representative atlas that can support the flexible generation of the required image operators for any selected optode arrangement. To facilitate accurate generation and mapping of DOT findings, we have developed an anatomical atlas-based method for DOT human brain imaging. In this report we extend this computation-efficient method to imaging studies of the brain of a Rhesus macaque. A hybrid Rhesus monkey brain atlas is generated by the substitution of a population-average MRI-based brain atlas of the rhesus macaque for an individual rhesus monkey whole head MRI scan. Evaluations from numerical simulation, phantom experiment and animal studies have shown that optode location, reconstruction of activation maps and mapping to the hybrid brain atlas can be made with high fidelity.

## Methods

For accurate generation and mapping of DOT findings, we have developed an anatomical atlas-based approach for human brain imaging [1,2]. One of the key elements of the method is the established MR-based FEM model library that contains FEM meshes from a selected MR atlas that has been segmented according to different tissue types and the pre-calculated imaging operators, as shown in Fig.1. Using synthetic data, we examined the accuracy with which image finding are mapped to the correct brain structures and subsequently are mapped to an individual's MR image [2].

In this report we extend the atlas-based method to imaging of the Rhesus monkey brain with DOT.

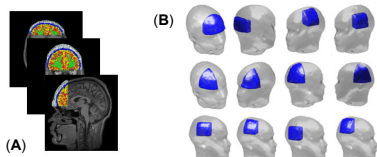


Figure 1. MRI-based segmented FEM brain mesh library.

**Generation of Hybrid Rhesus Brain Atlas:** To minimize subject bias, a hybrid brain atlas was generated by substitution of a population-averaged MRI-based brain atlas for the Rhesus macaque (112 monkeys: 80 males, 32 females available from the literature [3]), into the whole-head MRI of an individual monkey, (healthy, young male), as shown in Fig.2.

**FEM Mesh and Image Generator:** The hybrid map is segmented into into six main classes—skin, muscle, skull, cerebrospinal fluid, gray matter, and white matter—for the generation of 3D finite element method (FEM) mesh, and the image generators are computed by numerically solving photon the diffusion equation for assigned tissue coefficients. Fig.3 shows the segmented FEM mesh and a FEM model with 64 sources and 64 detectors.

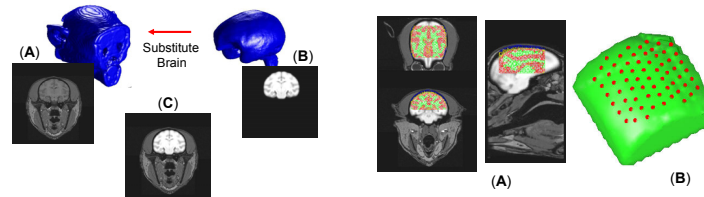


Figure 2. Hybrid brain atlas. (A) individual monkey head; (B) group averaged monkey brain; (c) hybrid monkey atlas.

Figure 3. (A) Segmented FEM mesh of an optical imaging region; (B) An FEM model with 64 sources and 64 detectors.

**Image Reconstruction:** 3D images of the Hb signal were reconstructed by using the normalized difference method [4]. This method solves a modified linear perturbation equation that is robust to many of the uncertainties common to experimental studies, including uncertainties associated with the initial guess, also known as the reference medium. Use of the linear approximation makes real-time 3D imaging feasible.

## Results

Qualitative and quantitative assessments of the fidelity of our method are presented in this section.

**Numerical Simulation:** Shown in Figure 4 is an example of our method applied to simulated data. Here an inclusion having a diameter of 1.0 cm was embedded at a mean depth of 1.2 cm and centrally located with respect to the position of a 30×30 source/detector array. The assigned absorption coefficient value ( $0.12 \text{ cm}^{-1}$ ) was twice that of the background;  $\mu_s^* = 10 \text{ cm}^{-1}$ . To mimic real experimental data, 2% Gaussian noise was added to simulated detector readings. Fig.4A shows the source/detector array and the inclusion position; Figs.4B and 4C are the inclusion positions and axial, coronal and sagittal sections (left to right) of the 3D reconstructed image, respectively. Careful inspection shows that the bias between the inclusion center and reconstructed image center is less than 2.5 mm.

**Phantom Experiment:** The reconstructed DOT images from experimental phantom data are presented in Fig.5. In this experiment a solid-state monkey phantom [5] containing a programmable  $1 \times 1 \times 0.2$  (cm) electrochromic (EC) cell, embedded in left posterior brain at a depth of 1 cm below the surface was used to mimic a spatiotemporal hemodynamic pattern of interest. Shown in Fig.5A are reconstructed total hemoglobin maps, where the location of EC cell is accurately recovered. The reconstructed signal and its PSD at the cell's position are shown in Figs.5B and 5C, illustrating excellent recovery of induced signal (1 Hz).

**Animal Experiment:** Fig.6 shows the results from an animal experiment data [6]. In the experiment, a macaque monkey was monitored using CW-NIRS DOT imager with probes placed on the mid frontal-parietal region of the exposed skull. An acute cerebral ischemia was induced via occlusion of the internal carotid and/or middle cerebral arteries, and subarachnoid bleeding was observed during the procedure. Post-surgical CT-scan, MRI and brain histopathology revealed concurrence between subarachnoid

bleeding, cortical ischemia, interventional procedures (contrast, vasodilator injection) and NIRS findings.

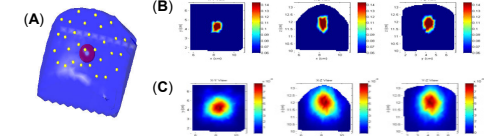


Figure 4. (A) 30x30 Source/detector array and inclusion; (B) Inclusion positions; (C) Reconstructed images.

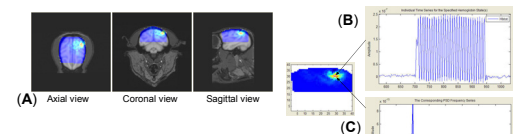


Figure 5. Results from phantom experimental data. (A) Reconstructed images; (B) Reconstructed signal; (C) Power spectral density distributions of reconstructed signal.

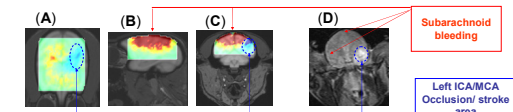


Figure 6. Results from animal experimental data. (A)-(C) Reconstructed total hemoglobin images; (D) MRI at the end of the experiment showing actual stroke area.

## Conclusion

In summary, we have developed an anatomical atlas-based method for generation and anatomical mapping of 3D DOT monkey brain image findings. As confirmed by numerical simulations, phantom and animal experimental data, our method is computation-efficient and is able to carry out anatomical mappings with high spatial and temporal accuracy. The reported capabilities have been integrated into our NAVI computing environment [7] to support model-based fNIRS reconstruction and generation of MR-based montages.

- [1] Y. Xu, Y. Pei, and R.L. Barbour, "An anatomical atlas-based method for efficient generation and registration of 3D DOT image findings," Paper NIH01-101 at The Inter-Institute Workshop on Optical Diagnostic and Biophotonic Methods from Bench to Bedside (Bethesda, MD, October 1-2, 2009).
- [2] Y. Xu, Y. Pei, and R.L. Barbour, "An anatomical atlas-based method for fNIRS tomography," Poster 864 MT-PM at the Meeting for Human Brain Mapping (Barcelona, Spain, June 6-10, 2010).
- [3] Donald G. McLaren, Kristopher J. Kosmatka, et al., "A population-average MRI-based atlas collection of the rhesus macaque," *NeuroImage* 45, pp. 52-59(2009).
- [4] Y. Pei, H.L. Graber, and R.L. Barbour (2001), "Influence of systematic errors in reference states on image quality and on stability of derived information for dc optical imaging," *Applied Optics*, 40, p. 5755.
- [5] R.L. Barbour, H.L. Graber, Y. Xu, et al., "A programmable laboratory testbed in support of evaluation of functional brain activation and connectivity," *IEEE Transactions on Neural Systems and Rehabilitation Engineering*, 20, 170-183(2012).
- [6] T. Gevorgyan, D.S. Pfeil, H.L. Graber, et al., "Cerebral monitoring during acute stroke and subarachnoid hemorrhage in the Bonnet Macaques with NIRS," Paper NIH100-52 at the 7th NIH Inter-Institute Workshop on Optical Diagnostic and Biophotonic Methods from Bench to Bedside (Bethesda, MD, September 15-16, 2011).
- [7] Y. Pei, Y. Xu, and R.L. Barbour, "NAVI-SciPort solution: A problem solving environment (PSE) for NIRS data analysis," Poster No. 221 M-AM at Human Brain Mapping 2007 (Chicago, IL, June 10-14, 2007).